Photodissociation of HBr. 1. Electronic Structure, Photodissociation Dynamics, and Vector Correlation Coefficients †

4 AUTHORS, INCLUDING:

Oleg S Vasyutinskii
Ioffe Physical Technical Institute
77 PUBLICATIONS   1,163 CITATIONS

SEE PROFILE

Gabriel Balint-Kurti
University of Bristol
186 PUBLICATIONS   4,670 CITATIONS

SEE PROFILE

Alex Brown
University of Alberta
87 PUBLICATIONS   1,363 CITATIONS

SEE PROFILE

Photodissociation of HBr. 1. Electronic Structure, Photodissociation Dynamics, and Vector Correlation Coefficients[†]

Andrey G. Smolin[‡] and Oleg S. Vasyutinskii[||]

Ioffe Physico-Technical Institute Russian Academy of Sciences, 194021 St.-Petersburg, Russia

Gabriel G. Balint-Kurti*

School of Chemistry, University of Bristol, Bristol BS8 1TS, United Kingdom

Alex Brown[§]

Department of Chemistry, University of Alberta, Edmonton, AB, T6G 2G2, Canada

Received: October 29, 2005

Ab initio potential energy curves, transition dipole moments, and spin−orbit coupling matrix elements are computed for HBr. These are then used, within the framework of time-dependent quantum-mechanical wave-packet calculations, to study the photodissociation dynamics of the molecule. Total and partial integral cross sections, the branching fraction for the formation of excited-state bromine atoms $Br(^2P_{1/2})$, and the lowest order anisotropy parameters, β, for both ground and excited-state bromine are calculated as a function of photolysis energy and compared to experimental and theoretical data determined previously. Higher order anisotropy parameters are computed for the first time for HBr and compared to recent experimental measurements. A new expression for the $Re[\mathbf{a}_1^{(3)}$ $(\|, \perp)]$ parameter describing coherent parallel and perpendicular production of ground-state bromine in terms of the dynamical functions is given. Although good agreement is obtained between the theoretical predictions and the experimental measurements, the discrepancies are analyzed to establish how improvements might be achieved. Insight is obtained into the nonadiabatic dynamics by comparing the results of diabatic and fully adiabatic calculations.

1. Introduction

   The photodissociation of hydrogen halides is important in the study of the atmospheric chemistry of the Earth and of other solar and stellar objects.[1−3] The process has been studied in recent years as a prototypical molecular dissociation exhibiting electronically nonadiabatic molecular dynamics, which becomes evident through the production of both excited and ground-state halogen atoms.[4−26] Of primary interest is the photodissociation process

$$HX + h\nu \rightarrow H(^2S) + X(^2P_{3/2})$$

$$\rightarrow H(^2S) + X(^2P_{1/2})$$
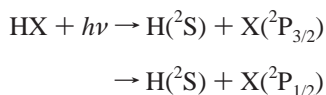
Often the halogen atom spin−orbit states are referred to as X and X* for the ground $X(^2P_{3/2})$ and excited $X(^2P_{1/2})$ state atoms, respectively. The first theoretical study of the competition or branching between the production of ground and electronically excited halogen atoms in this process was carried out by one of the authors[4] on an early calculated potential[27] for the HCl molecule. In this work, the spin−orbit coupling interactions were added to the computed potential energy curves in an empirical manner. The work showed clearly the importance of examining the energy dependence of the branching fraction for the production of the excited electronic state halogen atom fragment and demonstrated that if the hydrogen halide was initially vibrationally excited then the energy dependence of this branching fraction would display particularly interesting features. Most experiments have utilized fixed-frequency ultraviolet lasers to study these processes, and it is only in the very most recent experiments[15,16,18] that it has been possible to start studying the energy dependence of the branching fraction.

   The study of the polarization of the angular momentum of photofragments arising in photodissociation processes and the dependence of these properties on the scattering direction provides a complete description of the dynamics. These properties can be fully described by a spherical tensor expansion of the generalized scattering cross section.[28,29] This expansion gives rise to orientation and alignment parameters, $\mathbf{a}_Q^{(K)}(p)$, the complete set of which carry with them all possible information about the angular distribution of the alignment and orientation of the angular momentum in question. In the present case of the photodissociation of HBr, this would be the combined spin−orbit angular momentum of the Br atom or the spin angular momentum of the hydrogen atom. In the photodissociation of HCl[30] and HBr,[25] it has been shown, by using such analysis of the dissociation process, that highly polarized hydrogen atoms can be produced through the use of circularly polarized light.

   Ab initio theoretical studies of the photodissociation dynamics of HF[10] and HCl[11] and calculations of the associated orientation and alignment parameters have been published. Similar calcula-

tions for HI,[12,31] based on both empirical and ab initio electronic structure data have also appeared in the literature. In this paper, we present analogous calculations for the final halogen halide in this series, HBr.

The paper is organized as follows. In Section 2.1., new ab initio calculations of the potential energy curves, including spin−orbit coupling, and transition dipole moments are discussed. These represent the best HBr data available in the literature. The theory for the photodissociation dynamics is reviewed briefly in Section 2.2. Our theoretical results for the total cross-section, the excited-state bromine branching fraction, and the anisotropy parameter, β, are discussed and compared to experiment and previous computations in Section 3.1. In Section 3.2, we report the first determination of the anisotropy parameters for bromine atoms resulting from HBr dissociation and compare them to the experimental measurements of Rakitzis et al.[25,32] A short summary is given in Section 4.

2. Theory

The theoretical calculation of the photodissociation process involves two important parts: the determination of the underlying electronic structure, that is, potential energy curves (PECs), dipole moments, and nonadiabatic couplings, and the dynamical calculations from which the photodissociation cross sections, the branching fractions, and the orientation and alignment parameters of the atomic photofragments can be determined.

2.1. Ab Initio Determination of the Electronic Structure. There have been many previous theoretical studies of the ground state of HBr and its associated dipole moment.[33−35] However, the number of calculations of the excited states is limited.[14,36] Therefore, we have undertaken an ab initio investigation of the twelve electronic states, $X^1\Sigma^+$ (nondegenerate), $^1\Pi$ (double degenerate), $^3\Pi$ (sixfold degenerate) and $^3\Sigma^+$ (threefold degenerate), that correlate with the lowest energy asymptote $H(^2S) + Br(^2P)$. As in our previous work on the hydrogen halides,[8,11,12] these electronic states will be referred to as the *diabatic* basis. When spin−orbit coupling is taken into account in the electronic structure calculations, there are two dissociation channels $H(^2S_{1/2}) + Br(^2P_{3/2})$ and $H(^2S_{1/2}) + Br(^2P_{1/2})$ involving ground state and spin−orbit excited-state bromine, respectively. Eight adiabatic states, $X^1\Sigma_{0^+}$ (ground state), $A^1\Pi_1$ (two substates), $a^3\Pi_1$ (two substates), $a^3\Pi_2$ (two substates), and $a^3\Pi_{0^-}$, correlate with the lowest energy asymptote, while four states, $t^3\Sigma_1$ (two substates), $a^3\Pi_{0^+}$, and $t^3\Sigma_{0^-}$, correlate with the excited-state asymptote. The term symbols translate as a mixed Hund's case (a)/case (c) according to $^{2S+1}\Lambda_\Omega$. For Hund's case (c), Ω is the only good quantum number and the $^{2S+1}\Lambda$ labels designate the largest case (a) contribution within the Franck−Condon region. The adiabatic states of importance in the dynamics are the ground state $X^1\Sigma_{0^+}$ and seven optically accessible excited states, that is, the $A^1\Pi_1$, $a^3\Pi_1$, $a^3\Pi_{0^+}$, and $t^3\Sigma_1^+$ states. The electronic states, including spin−orbit coupling, will be later referred to as the *adiabatic* basis.

For the determination of the diabatic potential energy curves, the spin−orbit couplings, and the transition and permanent dipole moments, calculations have been performed using the MOLPRO program.[37] For bromine, the small-core relativistic pseudopotential and augmented correlation consistent polarized valence quintuple zeta basis set (aug-cc-pV5Z-PP)[38,39] was used. This corresponds to a (16s,13p,13d,3f,2g,1h)/[7s,6p,5d,3f,2g,1h] contraction. For the hydrogen atom, the aug-cc-pV5Z basis,[40] with the (9s5p3d2f1g)/[5s4p3d2f1g] contraction, was utilized.

A sequence of electronic structure calculations have been carried out to determine the molecular properties required for the dynamics, that is, potential energy curves, transition dipole moments, permanent dipole moments, and spin−orbit couplings. To determine the diabatic potential energy curves and permanent dipole moments, complete active space self-consistent field (CASSCF)[41,42] calculations were first performed for each state separately. The active space comprised the valence space only, that is, eight electrons in five orbitals. Multireference internally contracted configuration interaction (MRCI)[43,44] calculations were then carried out using the CASSCF orbitals and wave functions. The effect of higher order excitation was estimated using the Davidson correction.[45] The total number of contracted configurations was 121 518, 121 795, 73 671, and 121 671 for the $X^1\Sigma^+$, $A^1\Pi$, $a^3\Pi$, and $t^3\Sigma^+$ states, respectively.

The $A^1\Pi \leftarrow X^1\Sigma^+$ electronic transition moment was determined using a slightly different procedure than that used for the diabatic PECs because it is necessary to have a common set of orbitals and a well-defined wave function to describe both states involved. The state-averaged CASSCF (SA-CASSCF) method[41,42] was used for the $X^1\Sigma$ and $A^1\Pi$ states, and then MRCI calculations were performed to obtain the transition moment.

Finally, the spin−orbit matrix elements were determined using a procedure that differed from both the calculation of the diabatic PECs and the electronic transition dipole moment. The SA-CASSCF method was used to calculate a common set of orbitals for all of the states involved in the dynamics, that is, the $X^1\Sigma^+$, $A^1\Pi$, $a^3\Pi$, and $t^3\Sigma^+$ states. The spin−orbit matrix elements were then computed at the CASSCF level. The bromine atom fine-structure splitting, $E(^2P_{1/2}) - E(^2P_{3/2})$, was calculated to be 3536 cm^{-1}, which is within 4% of the experimental value[46] of 3685 cm^{-1}.

The adiabatic PECs are determined by diagonalizing a matrix containing the (diagonal) diabatic potential energy curves and the (off-diagonal) spin−orbit couplings. Both the adiabatic PECs and the matrix, $\mathbf{M}(R)$, which transforms from the diabatic to the adiabatic representation, are needed in order to perform the time-dependent wave-packet dynamics.[47,48] The adiabatic potential energy curves are illustrated in Figure 1. The states are labeled by the case (a) diabatic state making the largest contribution to the adiabatic state in the Franck−Condon region and by the quantum number Ω. The figure shows the adiabatic potentials for only the ground state and the optically accessible excited states, that is, $\Omega = 0^+$ and $\Omega = 1$ (all states shown being of e symmetry).[5,8] Using the transformation matrix $\mathbf{M}(R)$, together with the diabatic dipole moment and transition dipole moment curves, the adiabatic transition dipole moments can also be determined. Figure 2 illustrates the adiabatic transition dipole moments as a function of R. Unlike HF[8] and HCl,[11] where the initial excitation is dominated by the $A^1\Pi_1 \leftarrow X^1\Sigma_{0^+}$ transition, in HBr all optically allowed transitions can contribute. Although, as discussed in Section 3, the direct $t^3\Sigma_1 \leftarrow X^1\Sigma_{0^+}$ transition contributes only at high energy because of the relative positions of the potential energy curves (see Figure 1).

Figure 3 shows the calculated spin−orbit coupling matrix elements. The most interesting aspect highlighted by this figure is the rapid increase in magnitude of the spin−orbit matrix element $\langle ^3\Pi_{0^+}|H_{SO}|^1\Sigma^+\rangle$ as a function of H−Br internuclear separation around $R = 2.4$ bohr. The two $\Omega = 0^+$ states, both of which are of e symmetry, are mixed by the spin−orbit coupling interaction. At $R = 2.4$ bohr, however, the energy separation between the diabatic $^1\Sigma^+$ and $^3\Pi_{0^+}$ states is too great to allow them to mix effectively. We see that the adiabatic transition dipole moment connecting these states increases to a maximum around $R = 5$ bohr (see Figure 2). At this much larger
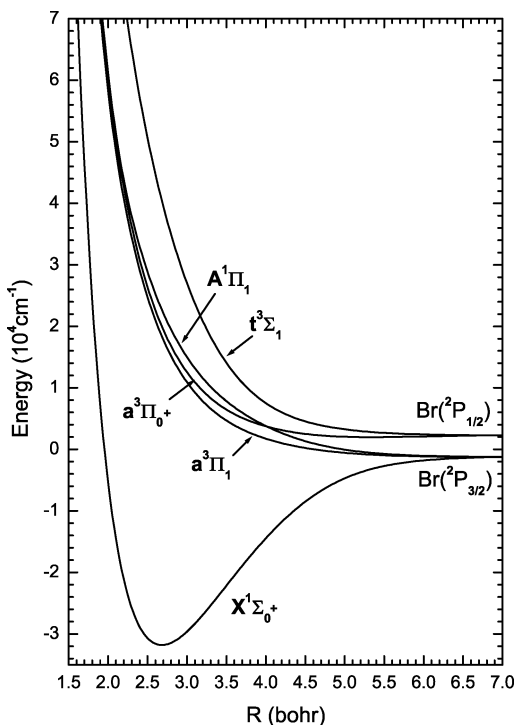
Photodissociation of HBr

J. Phys. Chem. A, Vol. 110, No. 16, 2006 **5373**

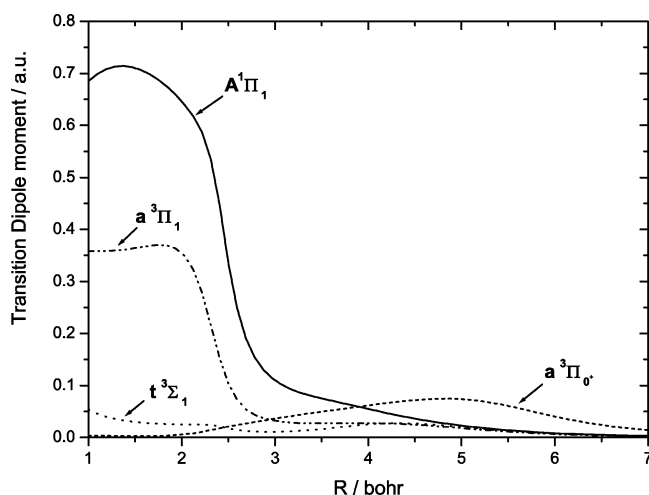**Figure 1.** Adiabatic potential energy curves as a function of the HBr internuclear distance.

Figure 2. Adiabatic transition dipole moments from the $X^1\Sigma_0^+$ ground electronic state to the four electronic states shown in Figure 1.

Figure 3. Spin−orbit coupling matrix elements as a function of the HBr internuclear distance, as determined by the CASSCF calculations.

bond length, the energy differences between the diabatic potential energy curves are now comparable to the magnitude of the spin−orbit coupling matrix element. Thus, at this larger bond length the diabatic states mix much more strongly. We will return to this discussion later in the paper.

The dissociation energy, D_0, calculated from the adiabatic $X^1\Sigma_0^+$ state is 29 316 cm^{-1} as compared to the experimental[18] value of 30 210 ± 40 cm^{-1}, the difference being 3.0%. The computed $X^1\Sigma_0^+$ ground state has also been used to determine the energies of the low-lying vibrational states of HBr by utilizing the Fourier grid Hamiltonian method.[49,50] Fitting to a simple anharmonic oscillator expression for the energies, the harmonic frequency, $\omega_e = 2636$ cm^{-1} and anharmonicity parameter $\omega_e x_e = 51.4$ cm^{-1} are in good agreement with the experimental values[51] of 2648.975 and 45.217 cm^{-1}, respectively. The good agreement of these calculated properties of
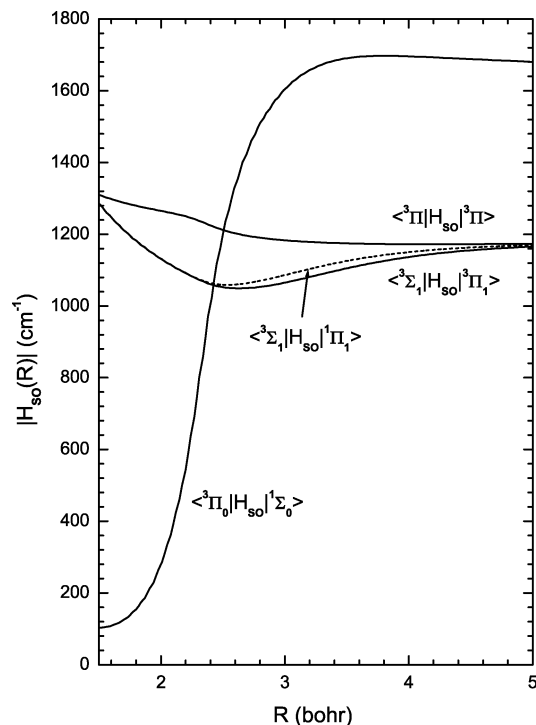
the ground-state electronic state potential energy curve with the corresponding experimental quantities is evidence of its accuracy.

2.2. Computation of the Photodissociation Dynamics. The photodissociation dynamics are computed using time-dependent quantum-mechanical wave-packet methods[8,11,12,47,48,52,53] based on the new ab initio potential energy curves, spin−orbit couplings, and dipole moments. Our first objective will be to test the quality of our ab initio calculations by comparing the computed scalar photodissociation properties, such as the total cross section and the Br($^2P_{1/2}$) branching fraction, with experimentally determined quantities. We will then compute the vector correlation and anisotropy parameters and compare these with measured quantities.

The computation of the anisotropy parameters from time-dependent wave-packet calculations of the dynamics has been well-documented[10,11] Here we review the pertinent information briefly. The photofragmentation **T** matrix elements are central to the calculation of the dynamical functions and anisotropy parameters.[10] For a diatomic molecule, AB, dissociating into atoms A and B, having angular momenta j_A and j_B, respectively, the dynamical functions $f_K(q, q')$ for fragment A are related to the **T** matrix elements as described in refs 10 and 12. The multipole rank,[12] K, of the dynamical functions for a photofragment with angular momentum j_A range from $K = 0$ to $K = 2j_A$. For the ground-state bromine fragment ($j_A = 3/2$), the complete set of the dynamical functions contains $K = 0, 1, 2$, and 3, whereas for the excited-state fragment ($j_A = 1/2$) only $K = 0$ and 1 are required. The anisotropy parameters, $a_Q^{(K)}(p)$,[54,55] are normalized combinations of the dynamical functions, where p refers to the symmetry of the transition connecting the ground electronic state to the dissociative excited states. Thus, p can be pure parallel (∥), pure perpendicular (⊥), or mixed parallel/perpendicular (∥, ⊥). These anisotropy parameters provide the most detailed information possible concerning the photodissociation dynamics.[12] The theoretical and experimental determination of these parameters is therefore the
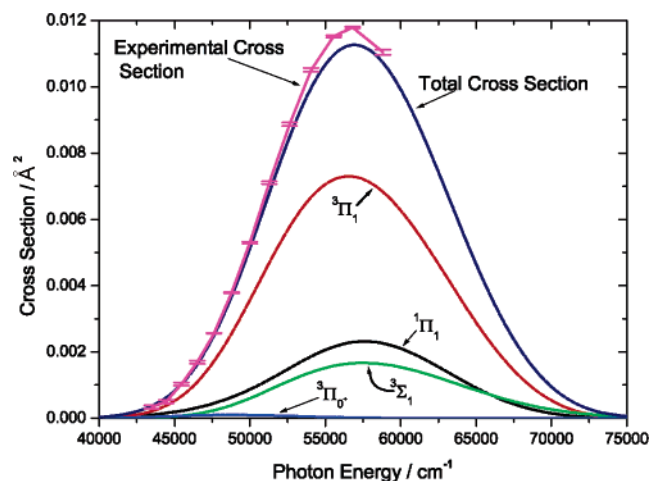
Figure 4. Theoretical and experimental[56] total cross-sections for the photodissociation of HBr. Also shown are the calculated partial cross sections. All calculated cross sections originate from the ground vibrational state.

best way to gain an in-depth understanding of the photodissociation dynamics.

For the ground-state bromine fragments, the $a_0^{(1)}$ ($\perp$), $a_0^{(2)}$ ($\perp$), $a_0^{(3)}$ ($\perp$), $a_2^{(2)}$ ($\perp$), $a_2^{(3)}$ ($\perp$), $a_1^{(1)}$ ($\parallel$, $\perp$), and $a_1^{(3)}$ ($\parallel$, $\perp$) anisotropy parameters are computed. For the excited-state bromine fragments, only the $a_1^{(1)}$ ($\parallel$, $\perp$) parameters are determined. The $a_0^{(K)}$ ($\perp$) parameters describe incoherent perpendicular excitation, the $a_2^{(K)}$ ($\perp$) parameters describe coherent perpendicular excitation, and the $a_1^{(K)}$ ($\parallel$, $\perp$) parameters, with $K = 1$ and 3, describe coherent parallel and perpendicular excitation. No parallel only parameters, $a_Q^{(K)}$ ($\parallel$), are computed because only a single state accessed by parallel excitation correlates with both the ground and excited-state asymptotes, and, therefore, these parameters are zero. An expression for the anisotropy parameter $a_1^{(3)}$ ($\parallel$, $\perp$) in terms of the dynamical functions[10] is given in the appendix because this has not been published previously.

3. Results and Discussion

3.1. Cross-Sections, Branching Fractions, and β Parameters. Figure 4 shows the total integral cross sections for the photodissociation of HBr from its ground vibrational state. The figure also shows the experimentally measured cross section of Huebert and Martin.[56] Our calculated total integral cross section compares quite well to the one measured experimentally, peaking at the same position and differing in magnitude by 4.4% at the peak of the cross section. The quoted error in the experimental cross section is only 0.18%. Although this is probably reliable, we note that the cross section differs by 9% from the closest experimental cross section measured by Goodeve and Taylor[57] 33 years earlier. The figure also shows the partial cross-sections. Surprisingly, the $a^3\Pi_1$ partial cross section, which arises from an electronically nonadiabatic transition from the $A^1\Pi_1$ state, makes the largest contribution to the total cross section, while both the $A^1\Pi_1$ and $t^3\Sigma_1$ partial cross sections make substantial contributions.

Figure 5 shows the results of a calculation of the partial and total cross sections using only the adiabatic curves and leaving out the nonadiabatic coupling matrix elements. The results of this calculation are informative because they show the effect of nonadiabatic transitions on the cross sections. The partial cross section to $t^3\Sigma_1$ is so small that it cannot be seen on the
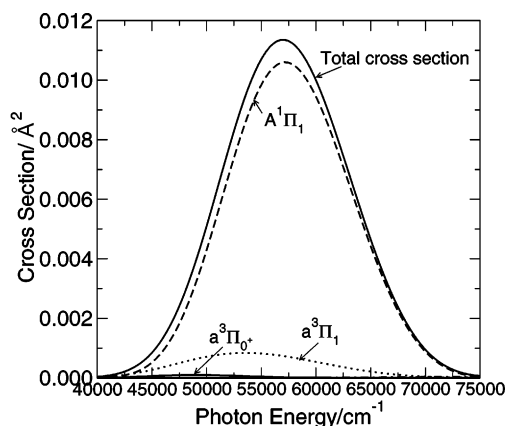

Figure 5. Theoretical total and partial cross-sections for the photodissociation of HBr as determined from an adiabatic calculation (see the text for details).
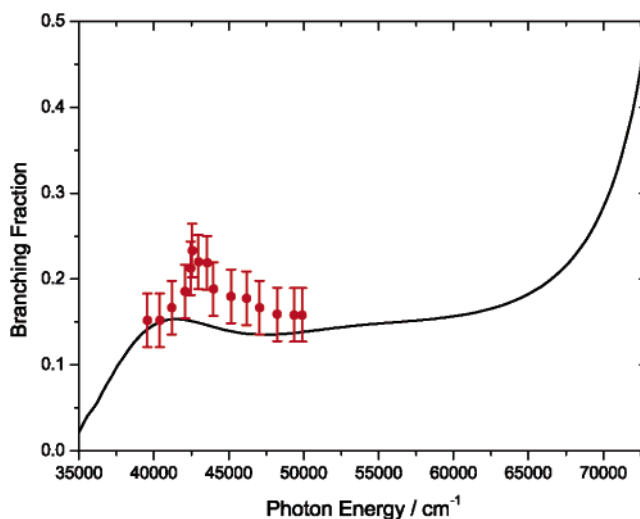

Figure 6. Excited-state Br atom branching fraction, $\Gamma = \sigma(\text{Br*})/(\sigma(\text{Br}) + \sigma(\text{Br*}))$, as a function of photon energy for the photodissociation of HBr. Results are from the present time-dependent wave-packet calculations (solid line) and the experimental measurements[18] (filled circles).

scale of the figure. This clearly demonstrates that the $t^3\Sigma_1$ state cannot be populated via direct excitation at any of the photon energies of interest. The contribution of the $A^1\Pi_1$ partial cross section to the total cross section is much greater, and those of the $a^3\Pi_1$ and $t^3\Sigma_1$ are less than the corresponding partial cross sections of the full calculation (including nonadiabatic dynamics). At 193 nm, the different adiabatic states make relative direct contributions of 89% ($A^1\Pi_1$), 10% ($a^3\Pi_1$), and 1% ($a^3\Pi_{0^+}$) to the total cross section. Rakitzis et al.[25] have assumed a contribution of 100% from adiabatic excitation to the $A^1\Pi_1$ state and have based their estimation of nonadiabatic transition probabilities of 0.80 and 0.14 to the $a^3\Pi_1$ and $t^1\Sigma_1$ states on this assumption. It would seem appropriate to reassess this analysis in the light of our calculations.

Figure 6 shows the Br atom excited-state branching fraction, $\Gamma = \sigma(\text{Br*})/(\sigma(\text{Br*}) + \sigma(\text{Br}))$, as a function of photon energy for the photodissociation of HBr from its lowest vibrational state. The figure also shows the experimental results of Regan et al.[18] The agreement between the calculated and experimental branching fraction as a function of photon energy is quite good. Although both the experimental and the theoretical branching fractions show a definite maximum as a function of energy, the position of the calculated maximum is at 41 000 cm^{-1}, whereas that of the experimental maximum is at 43 000 cm^{-1}.

Photodissociation of HBr

J. Phys. Chem. A, Vol. 110, No. 16, 2006 **5375**

TABLE 1: Anisotropy Parameters Obtained for Br(^2P_J) at 193 nm[a]

parameter	Br($^2P_{3/2}$)		Br($^2P_{1/2}$)	
	experiment (ref)	theory	experiment (ref)	theory
β	-0.88 ± 0.10 (32)		-0.21 ± 0.10 (25)	
	-1.0 (22)	-0.99	-1.0 (22)	-0.78
	-0.9 ± 0.10 (26)		0.00 ± 0.10 (26)	
$a_0^{(1)}(\perp)$	0.30 ± 0.07 (25)	0.35	0.55 ± 0.16 (25)	0.577
$a_0^{(2)}(\perp)$	-0.7 ± 0.2 (32)	-0.51	$\cdots$	$\cdots$
$a_2^{(2)}(\perp)$	-0.3 ± 0.2 (32)	-0.29	$\cdots$	$\cdots$
Re[$a_1^{(1)}(\|, \perp)$]	0.09 ± 0.08 (25)	0.031	0.46 ± 0.16 (25)	0.36

[a] References for the experimental measurements are given in brackets.

The previous theoretical calculations[7] did not predict a maximum in the branching fraction; in fact, they found a shallow minimum near 44 000 cm^{-1}. The form of the experimental maximum seems to be "cusped," whereas the maximum in the theoretical curve is smooth. Regan et al.[18] suggested that the presence of the "cusp" is due to a cooperative effect between the two mechanisms producing excited-state bromine atoms: (1) dissociation via a direct parallel transition to the a$^3\Pi_{0^+}$ state and (2) dissociation through a perpendicular mechanism via the t$^3\Sigma_1$ state, which is populated by nonadiabatic coupling from the A$^1\Pi_1$ and a$^3\Pi_1$ states; it cannot be populated via direct excitation at these low photon energies, see Figures 1 and 5. As we will see below, the theoretical calculations confirm that there is a change in mechanism for the production of Br* atoms from parallel to perpendicular absorption as the photon energy increases. The photon energy at which this change occurs is very sensitive to the computed relative energies of the a$^3\Pi_{0^+}$ and t$^3\Sigma_1$ states, the transition dipole moment to a$^3\Pi_{0^+}$, and nonadiabatic couplings resulting in population of t$^3\Sigma_1$ at these low photon energies. Hence, although the current ab initio calculations are very good (see Section 2.1 and the subsequent discussion in Section 3.2), they are still insufficient to reproduce the details of the experimentally observed "cusp."

3.2. Anisotropy Parameters for Br($^2P_{3/2}$) and Br($^2P_{1/2}$). The full set of anisotropy parameters describing the orientation and alignment of Br($^2P_{3/2}$) and Br($^2P_{1/2}$) atomic fragments was computed over a wide range of photolysis wavelengths. Many of these parameters have been measured experimentally at 193 nm by Rakitzis et al.,[25,32] and we compare our calculated values with these measurements in Table 1. Two other experimental measurements[22,26] of the anisotropy parameter, β, at 193 nm for both product channels are also included in the table.

As may be seen from the partial cross sections in Figure 4, the vast majority of the photofragmentation process occurs via a perpendicular transition (see curves marked A$^1\Pi_1$, a$^3\Pi_1$, and t$^3\Sigma_1$). These pathways give rise to a β parameter of -1. All of the adiabatic curves correlating with ground-state Br atoms arise from $\Omega = 0 \rightarrow \Omega = 1$ transitions (see Figure 1). Any parallel contribution to the anisotropy parameter, β, for ground-state Br atoms must therefore arise from a nonadiabatic transition during the breakup process. The calculated value of the anisotropy parameter for the ground state Br fragment is nearly -1.0 at all photon energies. This value of $\beta \approx -1.0$ is in agreement with experimental measurements of Regan et al.[18] at $\lambda = 203$, 213, 222, 233, and 243.1 nm and of Xu et al.[22] at 193 nm. Rakitzis et al.[32] measures $\beta = -0.88 \pm 0.05$ at 193 nm, and Baumfalk et al.[26] find values of β equal to -0.9 ± 0.10, -0.82 ± 0.30, and -0.96 ± 0.05 at wavelengths of 193, 205, and 243 nm, respectively. Therefore, except for the recent
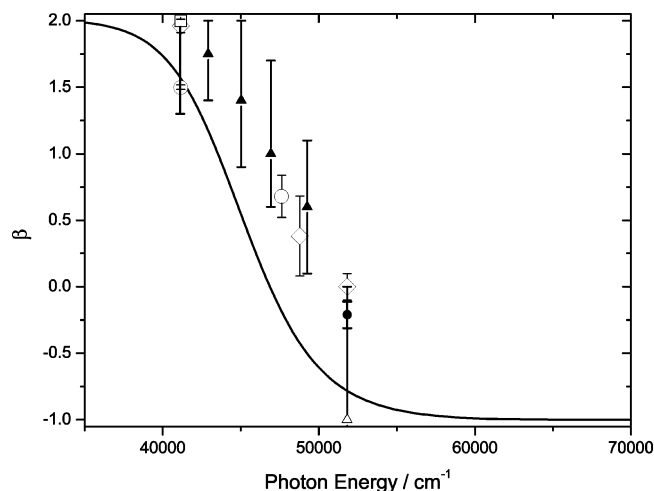

Figure 7. Anisotropy parameters, β, for the excited Br* (solid line) fragment as a function of photon energy for the photodissociation of HBr excited from its ground $v = 0$ state. Also shown are the experimental measurements from ref 18 (filled triangles), ref 22 (open triangles), ref 24 (open squares), ref 25 (filled circle), ref 26 (open diamonds), and ref 60 (open circles).

measurements of Rakitzis et al., we agree with all of the experimental measurements of the β parameter for the Br($^2P_{3/2}$) atomic fragment within the experimental error bars.

Figure 7 shows the calculated anisotropy parameter, β, for Br* atoms as a function of photon energy. Only two states, a$^3\Pi_{0^+}$ and t$^3\Sigma_1$ dissociate adiabatically to give Br* atoms. The partial cross section for the a$^3\Pi_{0^+}$ state corresponds to a parallel transition, whereas that for the t$^3\Sigma_1$ state corresponds to a perpendicular transition. At low excitation energies, the partial cross section for the a$^3\Pi_{0^+}$ state dominates and $\beta = 2$, corresponding to a parallel transition, whereas at higher energies the partial cross section for t$^3\Sigma_1$ dominates and $\beta = -1$. Similar behavior is seen in the calculated anisotropy parameter for excited-state iodine atoms produced from the analogous HI molecule.[31] Figure 7 also shows experimentally measured values[18,22,24−26,60] of β, for the H + Br* products. The general form of the calculated β versus photon energy curve agrees well with the experimentally measured values, but the calculated transition from a parallel to perpendicular photodissociation process occurs at a slightly too low photon energy. The parallel transition amplitude is much smaller in the analogous HF[8] and HCl[11] systems. It arises entirely through the spin−orbit mediated mixing of the diabatic X$^1\Sigma_0^+$ and a$^3\Pi_{0^+}$ states. As discussed in Section 3.1 with regard to the Br* branching fraction, the exact photon energy at which the photodissociation process to produce Br* changes from parallel to perpendicular is very sensitive to the details of the electronic structure for the a$^3\Pi_{0^+}$ and t$^1\Sigma_1$ states (i.e., the positions of the potential energy curves, the couplings between them, and the transition dipole moment to the a$^3\Pi_{0^+}$ state).

Figure 8 illustrates the anisotropy parameters describing incoherent perpendicular excitation, $a_0^{(K)}(\perp)$, for the ground-state Br($^2P_{3/2}$) photofragments from the photodissociation of HBr as a function of photolysis wavelength. The results are for excitation from the $v = 0$ vibrational state. These parameters provide information about the relative yields on the A$^1\Pi_1$ and a$^3\Pi_1$ electronic states;[10] information that cannot be accessed via the measurement of the total cross-section, branching fraction, or β parameter. The agreement between the theoretical and experimental result[25] at 193 nm for $a_0^{(1)}(\perp)$ for HBr is
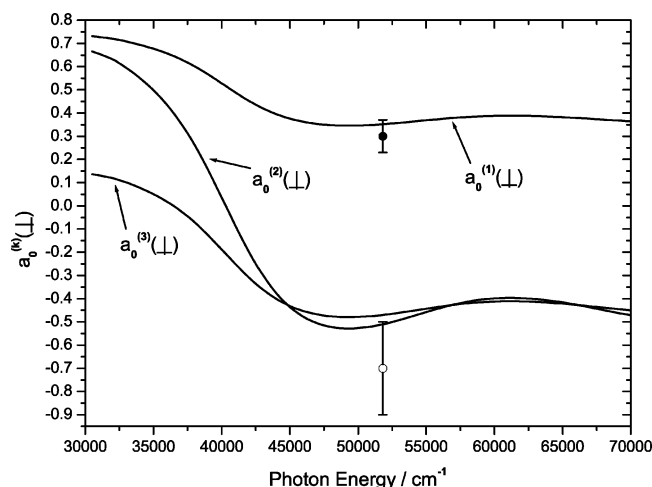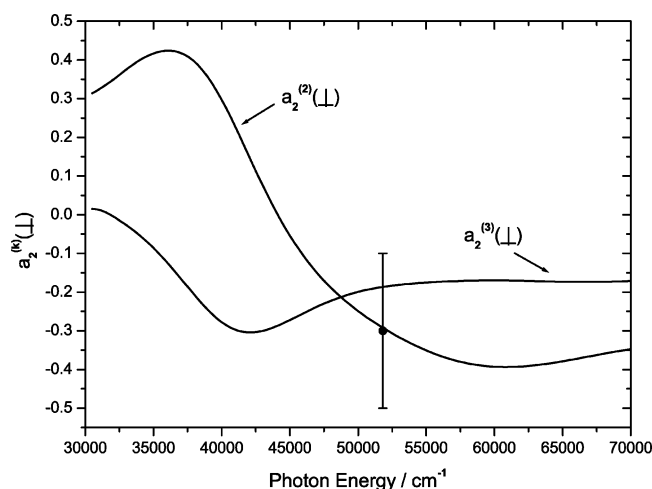
Figure 8. Incoherent anisotropy parameters $a_0^{(K)}$ ($\perp$) for the production of ground-state Br($^2P_{3/2}$) atoms as a function of photon energy following the photodissociation of HBr (solid lines) excited from its ground vibrational state. Also shown are the experimental measurements for $\mathbf{a}_0^{(1)}$ ($\perp$) (●) and $\mathbf{a}_0^{(2)}$ ($\perp$) (○) of Rakitzis et al.[25] at 193 nm.

Figure 10. Coherent anisotropy parameters $\text{Re}[\mathbf{a}_1^{(1)}$ (∥, $\perp$)] and $\text{Im}[\mathbf{a}_1^{(1)}$ (∥, $\perp$)] for the production of ground-state Br($^2P_{3/2}$) atoms as a function of photon energy following the photodissociation of HBr (solid lines) excited from its ground, $v = 0$, vibrational state. Also shown is the experimental measurement of $\text{Re}[\mathbf{a}_1^{(1)}$ (∥, $\perp$)] (●) of Rakitzis et al.[25] for HBr at 193 nm.

Figure 9. Coherent anisotropy parameters $\mathbf{a}_2^{(K)}$ ($\perp$) for the production of ground-state Br($^2P_{3/2}$) atoms as a function of photon energy following the photodissociation of HBr (solid lines) excited from its ground, $v = 0$, vibrational state. Also shown is the experimental measurement of Rakitzis et al.[25] for $\mathbf{a}_2^{(2)}$ ($\perp$) (●) at 193 nm.

Figure 11. Coherent anisotropy parameter $\text{Re}[\mathbf{a}_1^{(3)}$ (∥, $\perp$)] for the production of ground-state Br($^2P_{3/2}$) atoms as a function of photon energy following the photodissociation of HBr (solid lines) excited from its ground, $v = 0$, vibrational state. Also shown is the experimental measurement of Rakitzis et al.[25] (●). Note that as our definition of the rank 3 anisotropy parameters is twice as large as that used by Rakitzis et al. (see appendix). We have divided our calculated parameter by two so as to provide a valid comparison with the measured value.

excellent and the theoretical value for the $\mathbf{a}_0^{(2)}$ ($\perp$) parameter also agrees with experiment[32] within the experimental uncertainty.

The calculated $\mathbf{a}_2^{(K)}$ ($\perp$) parameters are shown in Figure 9. These parameters describe the coherent perpendicular excitation of the $a^3\Pi_1$ and $A^1\Pi_1$ states. The agreement between theory and experiment[32] for $\mathbf{a}_2^{(2)}$ ($\perp$) is again excellent. Parameter $\mathbf{a}_2^{(2)}$ ($\perp$) describes the degree of coherence between Br($^2P_{3/2}$) atoms in states with their z component of the angular momentum associated with quantum numbers m and $m \pm 2$.

The $\mathbf{a}_1^{(1)}$ (∥, $\perp$) parameter describing the coherent parallel and perpendicular excitation for ground-state Br($^2P_{3/2}$) is presented in Figure 10 as a function of photon energy. This parameter provides information about the interference between dissociation arising from parallel absorption pathways (i.e., dissociation on the X $^1\Sigma_0$ state potential curve populated from $a^3\Pi_0$ by nonadiabatic coupling) and dissociation arising from perpendicular absorption pathways (i.e., dissociation on the $A^1\Pi_1$ and $a^3\Pi_1$ potential curves). Any deviation of the $\mathbf{a}_1^{(1)}$ (∥, $\perp$) parameter from zero indicates a (minor) parallel
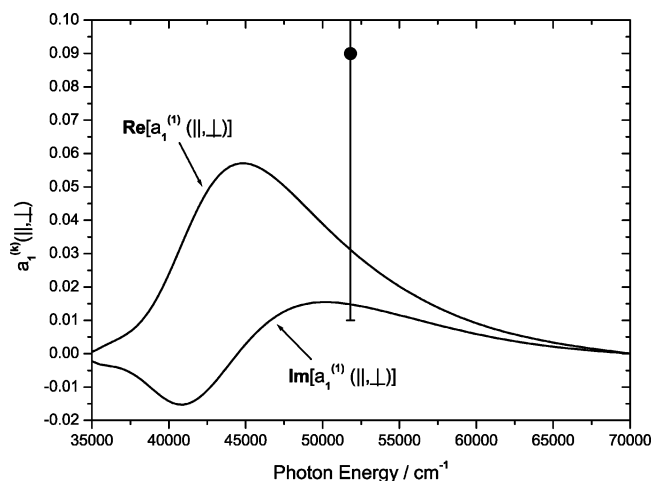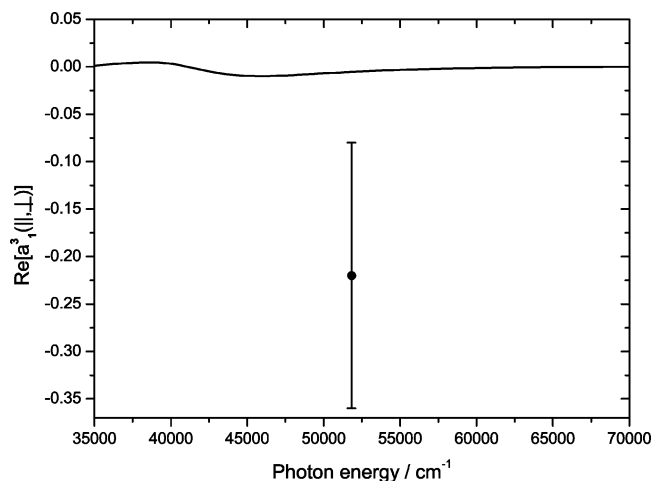
component and, therefore, the presence of a nonadiabatic transition from $a^3\Pi_0$ to the X $^1\Sigma_0$ ground state. The theoretical results agree with experiment within the experimental uncertainty.

The real part of the $\mathbf{a}_1^{(3)}$ (∥, $\perp$) anisotropy parameter is shown in Figure 11 and is compared to the experimental value quoted by Rakitzis et al.[25] The calculated value falls just outside the rather large error bars assigned to the experimental measurement. Note, however, that several assumptions were made in the analysis of the experimental results,[25] which might lead to an incorrect value for the $\mathbf{a}_1^{(3)}$ (∥, $\perp$) parameter. The assumptions made involve assuming that several anisotropy parameters, including in particular parameter $\mathbf{a}_2^{(3)}$ ($\perp$), may be ignored or set to zero so as to permit the extraction of other parameters from the experimental data. Our theoretical calculation of the $\mathbf{a}_2^{(3)}$ ($\perp$) parameter is presented in Figure 9, which shows that this parameter has a value of about -0.19 at 193 nm. This is
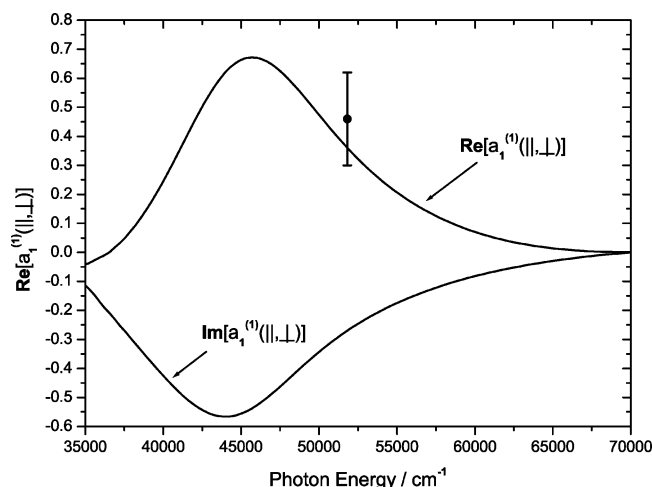
Photodissociation of HBr

J. Phys. Chem. A, Vol. 110, No. 16, 2006 **5377**

Figure 12. Coherent anisotropy parameters Re[$a_1^{(1)}$ (||, ⊥)] and Im[$a_1^{(1)}$ (||, ⊥)] for the production of excited-state Br($^2P_{1/2}$) atoms as a function of photon energy following the photodissociation of HBr (solid lines) excited from its ground, $v = 0$, vibrational state. Also shown is the experimental measurement of Re[$a_1^{(1)}$ (||, ⊥)] (●) of Rakitzis et al.[25] for HBr at 193 nm.

not an inconsiderable value, and setting this to zero in the analysis process might lead to errors. Alternative methods of analyzing such experimental data have been proposed by some of the authors.[58,59]

The polarization of excited-state Br($^2P_{1/2}$) photofragments is fully described by just ($K = 1$) orientation parameters, $a_0^{(1)}$ (⊥) and $a_1^{(1)}$ (||, ⊥). The $a_0^{(1)}$ (⊥) parameter is not plotted because it is constant and equal to its maximal value of 0.577 (= $1/\sqrt{3}$), while the $a_1^{(1)}$ (||, ⊥) parameter is illustrated in Figure 12. We see from the figure that the calculated value of the parameter agrees very well with the experimental[25] value at 193 nm. The Re[$a_1^{(1)}$ (||, ⊥)] and Im[$a_1^{(1)}$ (||, ⊥)] parameters are dependent on the phase difference of the radial wave functions created on the $a^3\Pi_{0^+}$ and $t^3\Sigma_1$ states modulated by the corresponding transition dipole moments to these states. In light of the photon energy dependence observed for the β parameter, see Section 3.1, we might anticipate that the peaks in the exact $a_1^{(1)}$ (||,⊥) curves would be shifted to somewhat higher photon energies than those shown in Figure 12.

4. Conclusions

We have presented new calculations of the potential energy curves, transition dipole moments, and spin−orbit coupling matrix elements for the low-lying electronic states of the HBr molecule. We have used the electronic structure data to examine the photofragmentation of HBr in the ultraviolet spectral region. Although there have been previous ab initio calculations of this photodissociation process,[7,14] our paper is the first that reports a comparison of the calculated and experimental absolute value of the photodissociation cross section for the system. As demonstrated in Figure 4, our calculated cross section peaks at the same photon energy as the experimental cross section and differs by only a few percent in magnitude from it. This clearly demonstrates the basic reliability of our calculations.

We also present the branching fraction for the production of Br* atoms. We compare these with the available experimental results[18,22,26,32] and find that there is a reasonable level of agreement (see Figure 6). The calculated values agree with the experimental ones to within the experimental uncertainty for about half of the measured points and lying just outside the

quoted experimental error bars for the other points. The experimental branching fraction curve seems to display a cusp that is absent from the theoretical curve; although the theory predicts a maximum at nearly the same wavelength as the cusp.

The anisotropy and vector correlation and alignment parameters for the system are also presented and discussed. Unlike in the case of HF[8,10] and HCl,[11] the increased spin−orbit coupling present in the case of HBr leads to a more readily measured parallel component of the photodissociation cross section (see Figures 2, 4 and 7). The predicted parallel component is, however still very small and is highly sensitive to the finer details of the electronic structure calculations. One consequence of this sensitivity is that the anisotropy parameter, β, for the excited Br* atom changes from that of a parallel to that corresponding to a perpendicular transition at slightly too low a photon energy as compared to the experimental measurements (see Figure 7).

Nearly all of the computed vector correlation and alignment parameters are found to agree with the few existing measurements of Rakitzis et al.[25] within the experimental error.

Appendix

Expressions for Anisotropy Parameter $a_1^{(3)}$ (||, ⊥) in Terms of Dynamical Functions. The relationship between the anisotropy parameters $a_Q^{(K)}$ and the dynamical functions, and the evaluation of the dynamical functions themselves, have been discussed in a previous papers.[10,11] Below we give an expression for the anisotropy parameter $a_1^{(3)}$, which has not been published previously.

$$a_1^{(3)}(||, \perp) = -\frac{2\sqrt{42}}{5}\frac{f_3(1,0)}{f_0(0,0) + 2f_0(1,1)} \quad (1)$$

The definition of the dynamical functions, $f_K(q, q')$ has been given by Balint-Kurti et al.,[10] where the evaluation of these functions is also discussed. Note that our definition of the anisotropy parameters of rank 3, as in the above equation, are larger by a factor of 2 than those used by Rakitzis et al.[25]

References and Notes

(1) Mahieu, E.; Zander, R.; Duchatelet, P.; Hannigan, J. W.; Coffey, M. T.; Mikuteit, S.; Hase, F.; Blumenstock, T.; Wiacek, A.; Strong, K.; Taylor, J. R.; Mittermeier, R. L.; Fast, H.; Boone, C. D.; McLeod, S. D.; Walker, K. A.; Bernath, P. F.; Rinsland, C. P. *Geophys. Res. Lett.* **2005**, *32*, L15S08.
(2) Jura, M. *Astrrophys. J. Lett.* **1974**, *190*, l33.
(3) Black, J. H.; Dalgarno, A. *Astrophys. J. Suppl.* **1977**, *34*, 405.
(4) Givertz, S. C.; Balint-Kurti, G. G. *J. Chem. Soc., Faraday Trans.* **1986**, *82*, 1231.
(5) Alexander, M. H.; Pouilly, B.; Duhoo, T. *J. Chem. Phys.* **1993**, *99*, 1752.
(6) Duhoo, T.; Pouilly, B. *J. Chem. Phys.* **1995,** *103*, 182.
(7) Peoux, G.; Monnerville, M.; Duhoo, T.; Pouilly, B. *J. Chem. Phys.* **1997**, *107*, 70.
(8) Brown, A.; Balint-Kurti, G. G. *J. Chem. Phys.* **2001**, *113*, 1870.
(9) Brown, A.; Balint-Kurti, G. G. *J. Chem. Phys.* **2001**, *113*, 1879.

Smolin et al.

(10) Balint-Kurti, G. G.; Orr-Ewing, A. J.; Beswick, J. A.; Brown, A.; Vasyutinskii, O. S. *J. Chem. Phys.* **2002**, *116*, 10760.

(11) Brown, A.; Balint-Kurti, G. G.; Vasyutiniskii, O. S. *J. Phys. Chem. A* **2004**, *108*, 7790.

(12) Brown, A. *J. Chem. Phys.* **2005**, *122*, 084301.

(13) Alekseyev, A. B.; Liebermann, H. P.; Kokh, D. B.; Buenker, R. J. *J. Chem. Phys.* **2000**, *113*, 6174.

(14) Pouilly, B.; Monnerville, M. *Chem. Phys.* **1998**, *238*, 437.

(15) Langford, S. R.; Regan, P. M.; Orr-Ewing, A. J.; Ashfold, M. N. R. *Chem. Phys.* **1998**, *231*, 245.

(16) Lambert, H. M.; Dagdigian, P. J.; Alexander, M. H. *J. Chem. Phys.* **1998**, *108*, 4460.

(17) Zhang, J.; Dulligan, M.; Wittig, C. *J. Chem. Phys.* **1997**, *107*, 1403.

(18) Regan, P. M.; Langford, S. R.; Orr-Ewing, A. J.; Ashfold, M. N. R. *J. Chem. Phys.* **1999**, *110*, 281.

(19) van Veen, G. N. A.; Mohamed, K. A.; Baller, T.; deVries, A. E. *Chem. Phys.* **1983**, *80*, 113.

(20) Magnotta, F.; Nesbitt, D. J.; Leone, S. R. *Chem. Phys. Lett.* **1981**, *80*, 21.

(21) Xu, Z.; Koplitz, B.; Wittig, C. *J. Chem. Phys.* **1987**, *87*, 1062.

(22) Xu, Z.; Koplitz, B.; Wittig, C. *J. Phys. Chem.* **1988**, *92*, 5518.

(23) Matsumi, Y.; Tonokura, K.; Kawasaki, M.; Ibuki, T. *J. Chem. Phys.* **1990**, *93*, 7981.

(24) Kinugawa, T.; Arikawa, T. *J. Chem. Phys.* **1992**, *96*, 4801.

(25) Rakitzis, T. P.; Samartzis, P. C.; Toomes, R. L.; Kitsopoulos, T. N. *J. Chem. Phys.* **2004**, *121*, 7222.

(26) Baumfalk, R.; Buck, U.; Frischkorn, C.; Nahler, N. H.; Hüwel, L. *J. Chem. Phys.* **1999**, *111*, 2595.

(27) van Dishoeck, E.; van Hemert, M.; Dalgarno, A. *J. Chem. Phys.* **1982**, *77*, 3693.

(28) Orr-Ewing, A. J.; Zare, R. N. *Annu. Rev. Phys. Chem.* **1994**, *45*, 315.

(29) Bracker, A. S.; Wouters, E. R.; Suits, A. G.; Lee, Y. T.; Vasyutinskii, O. S. *Phys. Rev. Lett.* **1998**, *80*, 1626.

(30) Rakitzis, T. P.; Samartzis, P. C.; Toomes, R. L.; Kitsopoulos, T. N.; Brown, A.; Balint-Kurti, G. G.; Vasyutinskii, O. S.; Beswick, J. A. *Science* **2003**, *300*, 1936.

(31) Jodoin, D. N.; Brown, A. *J. Chem. Phys.* **2005**, *123*, 054301.

(32) Rakitzis, T. P.; Samartzis, P. C.; Toomes, R. L.; Tsigaridas, L.; Coriou, M.; Chestakov, D.; Eppink, A. T. J. B.; Parker, D. H.; Kitsopoulos, T. N. *Chem. Phys. Lett.* **2002**, *264*, 115.

(33) Čížek, M.; Horáček, J.; Sergenton, C.; Popovič, D.; Allan, M.; Domcke, W.; Leininger, T.; Gadea, F. *Phys. Rev. A* **2001**, *63*, 062710.

(34) Seth, M.; Fischer, T.; Schwerdtfeger, P. *J. Chem. Soc., Faraday Trans.* **1996**, *92*, 167.

(35) Werner, H.-J.; Rosmus, P. *J. Chem. Phys.* **1980**, *73*, 2319.

(36) Chapman, D. A.; Balasubramanian, K.; Lin, S. H. *Chem. Phys.* **1987**, *118*, 333.

(37) MOLPRO is a package of ab initio programs written by Werner, H.-J.; Knowles, P. J.; Schtz, M.; Lindh, R.; Celani, P.; Korona, T.; Rauhut, G.; Manby, F. R.; Amos, R. D.; Bernhardsson, A.; Berning, A.; Cooper, D. L.; Deegan, M. J. O.; Dobbyn, A. J.; Eckert, F.; Hampel, C.; Hetzer, G.; Lloyd, A. W.; McNicholas, S. J.; Meyer, W.; Mura, M. E.; Nickla, A.; Palmieri, P.; Pitzer, R.; Schumann, U.; Stoll, H.; Stone, A. J.; Tarroni, R.; Thorsteinsson, T.

(38) Peterson, K.; Figgen, D.; Goll, E.; Stoll, H.; Dolg, M. *J. Chem. Phys.* **2003**, *119*, 11113.

(39) Basis sets were obtained from the Extensible Computational Chemistry Environment Basis Set Database, Version 02/25/04, as developed and distributed by the Molecular Science Computing Facility, Environmental and Molecular Sciences Laboratory, which is part of the Pacific Northwest Laboratory, P.O. Box 999, Richland, WA 99352, and funded by the U.S. Department of Energy. The Pacific Northwest Laboratory is a multi-program laboratory operated by Battelle Memorial Institute for the U.S. Department of Energy under contract DE-AC06-76RLO 1830. Contact Karen Schuchardt for further information.

(40) Dunning, T. H., Jr. *J. Chem. Phys.* **1990**, *90*, 1007.

(41) Knowles, P. J.; Werner, H. J. *Chem. Phys. Lett.* **1985**, *115*, 259.

(42) Werner, H. J.; Knowles, P. J. *J. Chem. Phys.* **1985**, *82*, 5053.

(43) Werner, H. J.; Knowles, P. J. *J. Chem. Phys.* **1988**, *89*, 5803.

(44) Knowles, P. J.; Werner, H. J. *Chem. Phys. Lett.* **1988**, *145*, 514.

(45) Langhoff, S. R.; Davidson, E. R. *Int. J. Quantum Chem.* **1974**, *8*, 61.

(46) Moore, C. E. *Atomic Energy Levels*; U.S. Government Printing Office: Washington, D.C., 1971.

(47) Balint-Kurti, G. G.; Brown, A. Time-dependent wavepacket calculations for reactive scattering and photodissociation. In *Theory of Chemical Reaction Dynamics: Proceedings of the Nato Advanced Research Workshop on the Theory of Dynamics of Elementary Chemical Reactions*; Lagana, A.; Lendvay, G., Eds.; Kluwer Academic Publishers: Dordrecht, The Netherlands, 2004.

(48) Balint-Kurti, G. G.; Dixon, R. N.; Marston, C. C. *J. Chem. Soc., Faraday Trans.* **1990**, *86*, 1741.

(49) Marston, C. C.; Balint-Kurti, G. G. *J. Chem. Phys.* **1989**, *91*, 3571.

(50) Balint-Kurti, G. G.; Ward, C. L.; Marston, C. C. *Comput. Phys. Commun.* **1991**, *67*, 285.

(51) Huber, K. P.; Herzberg, G. *Molecular Spetra and Molecular Structure IV. Constants of Diatomic Molecules*; Van Nostrand: Princeton, NJ, 1979.

(52) Kulander, K. C.; Heller, E. J. *J. Chem. Phys.* **1978**, *69*, 2439.

(53) Heller, E. J. *Acc. Chem. Res.* **1981**, *14*, 368.

(54) Rakitzis, T. P.; Zare, R. N. *J. Chem. Phys.* **1999**, *110*, 3341.

(55) Rakitzis, T. P.; Hall, G.; Costen, M. L.; Zare, R. N. *J. Chem. Phys.* **1999**, *111,* 8751.

(56) Huebert, B. J.; Martin, R. M. *J. Phys. Chem.* **1968**, *72*, 3046.

(57) Goodeve, C. F.; Taylor, A. W. C. *Proc. R. Soc. London, Ser. A* **1935**, *152*, 221.

(58) Smolin, A. G.; Vasyutinskii, O. S.; Wouters, E. R.; Suits, A. G. *J. Chem. Phys.* **2004**, *121*, 1.

(59) Smolin, A. G.; Nahler, N. H.; Vasyutinskii, O. S.; Vieuxmaire, O. P. J.; Balint-Kurti, G. G.; Orr-Ewing, A. J.; Ashfold, M. N. R. *J. Chem. Phys.*, to be published.

(60) Shiell, R. C.; Hepburn, J. Private communication quoted in ref 26; D. L. Lacombe, M. Sc. thesis, University of Waterloo, Canada, 1997.